Elastic thickness estimates for coronae associated with chasmata on Venus

Trudi Hoogenboom[1] and Greg Houseman
School of Earth and Environment, University of Leeds, Leeds, UK

Paula Martin
Department of Physics, University of Cambridge, Cambridge, UK

Received 23 December 2004; revised 7 April 2005; accepted 14 April 2005; published 8 September 2005.

[1] In this study we investigate the relationship between the local elastic lithospheric thickness and the relative ages of coronae on Venus in an attempt to further understand corona and chasmata formation/evolution. We use Magellan gravity and topography data to estimate the elastic lithospheric thickness in the vicinity of coronae associated with chasmata. The relative timing of corona formation with respect to chasmata formation is classified using superposition relationships between fractures and flows associated with the corona, and the regional fracture sets associated with the chasmata. For the 31 coronae that we here examine (limited by low resolution of the Magellan gravity field in some regions of interest), estimates of elastic thickness appear to be related to the relative timing of corona formation. Coronae that formed after chasmata exhibit smaller values of elastic thickness (0 to 19 km), which may result from their formation on relatively warm and weak lithosphere due to lithospheric extension associated with chasmata formation. Coronae that formed prior to chasmata formation display greater elastic thickness values (0 to 56 km). These coronae are interpreted to have formed on lithosphere that was stronger (colder). However, examples of coronae with small elastic thickness (<5 km) are found in all relative timing groups.

Citation: Hoogenboom, T., G. Houseman, and P. Martin (2005), Elastic thickness estimates for coronae associated with chasmata on Venus, *J. Geophys. Res.*, *110*, E09003, doi:10.1029/2004JE002394.

1. Introduction

[2] First identified in Venera 15/16 images, coronae are large-scale tectonic structures described by *Barsukov et al.* [1984] as circular features surrounded by an annulus of ridges (e.g., Figures 1 and 3). They are generally considered unique to Venus and may offer insights into the differences in lithospheric structure or mantle convective pattern between Venus and Earth. Coronae are widely accepted as the surface expression of mantle diapirs [e.g., *Stofan et al.*, 1991; *Janes et al.*, 1992; *Squyres et al.*, 1992]. However, numerical models of their formation [e.g., *Koch and Manga*, 1996; *Smrekar and Stofan*, 1997] are unable to reproduce both the diameter and range of observed topographic profiles. In addition, the depth and nature of such mantle diapirs is uncertain [*Hansen*, 2003]. Coronae have also been suggested to result from Rayleigh-Taylor (gravitational) instability of the lithosphere [*Tackley and Stevenson*, 1991; *Hamilton and Stofan*, 1996; T. Hoogenboom and G. A. Houseman, Rayleigh-Taylor instability as a mechanism for coronae formation on Venus, submitted to *Icarus*, 2005].

[3] Most (68%) of the total population of coronae are associated with chasmata or fracture belts [*Stofan et al.*, 1997]. The remaining 32% are located at volcanic rises or as isolated features in the plains [*Stofan et al.*, 1997]. Chasmata are linear to arcuate troughs, with trough-parallel fractures and faults that extend for thousands of kilometers (Figure 1). They have previously been interpreted as extensional rift zones [*McGill et al.*, 1981; *Schaber*, 1982; *Solomon et al.*, 1992; *Jurdy and Stefanick*, 1999]. Alternatively some chasmata, located on the margins of the largest coronae features, have been interpreted as subduction trenches [*McKenzie et al.*, 1992; *Sandwell and Schubert*, 1992; *Schubert and Sandwell*, 1995] given the similarity of the topographic profiles and shapes of the trench to terrestrial island arcs (diagnostic of the subduction process on Earth). However, the subduction trench interpretation is disputed on the basis of geological mapping [*Hansen and Phillips*, 1993; *Hansen et al.*, 1997] and mantle temperature estimates [*Senft and Kiefer*, 2003].

[4] Estimates of the elastic thickness of the lithosphere (T_e), have been calculated in a number of gravity, topography and/or admittance studies of Venus [e.g., *Simons et al.*, 1997; F. S. Anderson and S. E. Smrekar, Global mapping of crustal and lithospheric thickness on Venus, submitted to *Journal of Geophysical Research*, 2005 (here-

[1]Now at Jet Propulsion Laboratory, Pasadena, California, USA.

0148-0227/05/2004JE002394$09.00

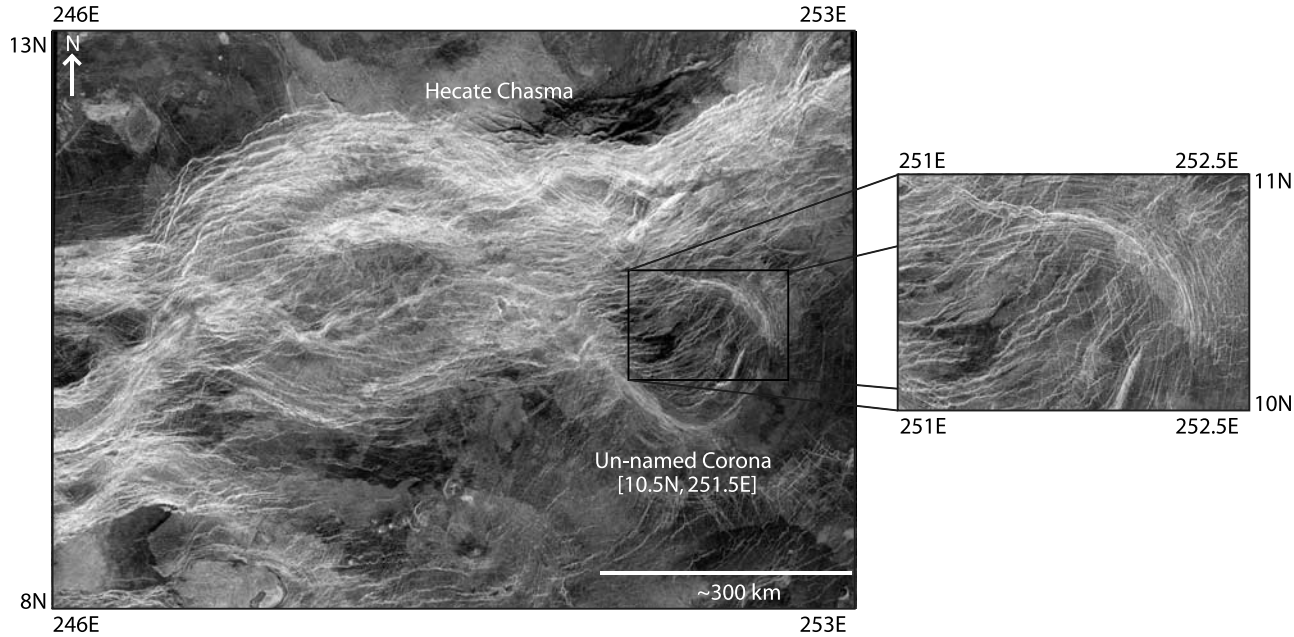

Figure 1. Magellan (left-looking) synthetic aperture radar (SAR) image (sinusoidal projection, image resolution: 1.2 km/pixel) of an unnamed corona (10.5N 251.5E) located on the main branch of the NE-SW trending Hecate Chasma (http://pdsmaps.wr.usgs.gov). Magellan SAR images are used in conjunction with full-resolution mosaic images (FMAPS) to interpret whether individual coronae formed prior to, during, or after chasmata formation. Relative timing of formation is established on the basis of superposition and cross-cutting relationships between coronae and regional fractures and volcanism. The unnamed corona (17 in Table 1) is classified syntectonic as chasmata-related fractures cut the corona flows, and some of the concentric corona fractures (in the N-NE of the corona) also superpose chasmata fractures as determined from the stereo images.

inafter referred to as Anderson and Smrekar, submitted manuscript, 2005)] and for coronae specifically [*Johnson and Sandwell*, 1994; *Schubert and Sandwell*, 1995; *Barnett et al.*, 2000, 2002; *Smrekar et al.*, 2003; *Hoogenboom et al.*, 2004]. None of these studies, however, have explored the dependence of lithospheric parameters on the tectonic history of the region, as implied from the interpretation of relative timing relationships between coronae and surrounding features. In this study, coronae closely associated with chasmata are classified according to their time of formation relative to the background tectonic deformation. These interpretations are then compared with elastic lithospheric thickness estimates derived from admittance spectra [*Hoogenboom et al.*, 2004]. Examining the relationship between the local elastic thickness of the lithosphere and the relative ages of coronae and chasmata may further constrain the origin and evolution of coronae and chasmata systems.

2. Methods

[5] The relative ages of coronae formation with respect to chasmata formation were classified by analysis of Magellan radar images. The relative ages of the coronae were then compared with estimates of local elastic thickness obtained by comparing the observed Magellan admittance functions with the predictions of flexural models [*Hoogenboom et al.*, 2004].

2.1. Elastic Thickness

[6] On Earth, the upper part of the lithosphere (30 km or less) behaves rigidly on long geological timescales. The main evidence for its rigidity comes from studies of the way the lithosphere responds elastically to surface loads. Elastic models are commonly used to estimate the elastic thickness of terrestrial lithosphere [e.g., *Watts et al.*, 1980; *McKenzie and Fairhead*, 1997]. The crust of Venus is believed to be composed primarily of basaltic material or the intrusive equivalent, diabase. In a recent set of experiments [*Mackwell and Kohlstedt*, 1993; *Mackwell et al.*, 1998], diabase samples were thoroughly dried before deformation (to approximate the arid, high-temperature conditions on Venus). These samples are more resistant to deformation than hydrated basalts [*Mackwell et al.*, 1998]. Water has a similar effect on the strength of olivine [*Karato et al.*, 1986]. Although the surface layers of Venus are much hotter than those of the Earth, the effect of dehydration may lead to effective elastic thicknesses comparable to those of Earth.

[7] The admittance spectrum (ratio of free-air gravity to topography in the spectral domain), is sensitive to bending of the elastic lithosphere in response to a load from above, below or both. We used a spatio-spectral localization method [*Simons et al.*, 1997] together with a global admittance map (Anderson and Smrekar, submitted manuscript, 2005) to calculate the local average spectral admittance function for the coronae listed in Table 1 as summarized by

Table 1. Coronae T_e Estimates Along With Location, Relative Age of Formation, Setting, Annulus Shape, and Maximum Diameter and the Flexural Model, Bottom- or Top-Loading, Used to Calculate T_e, Crustal Thickness Z_c, and Apparent Depth of Compensation Z_L[a]

Name	Lat.	Long	Annulus Shape	Max. Diam., km	Relative Age	Setting	Model	T_e, km	T_e Range, km 1.5	Z_c, km	Z_c Range, km 1.5	Z_L, km	Z_L Range, km 1.5	RMS Fit, mgal/km	RMS Obs., mgal/km
1. Tamiyo	−36.0	298.5	asymmetric	375	Pre	Parga	bottom	46	42–56	-	-	60	57–61	0.3	1.0
2.	5.0	225.0	concentric	450	Pre	Hecate	top	45	40–55	21	13–46	-	-	2.3	2.1
3.	17.8	240.0	concentric	350	Pre	Hecate	top	25	21–29	64	59–67	-	-	5.1	2.8
4. Sith	−10.2	176.5	asymmetric	450	Pre	Dali Diana	top	0	0–18	37	17–63	-	-	7.3	12.2
5. Prthivi	11.0	248.5	concentric	300	Syn/Pre	Hecate	top	47	40–56	47	39–57	-	-	2.7	2.1
6.	10.0	246.0	concentric-DR	200	Syn/Pre	Hecate	top	47	42–54	46	39–53	-	-	3.2	2.4
7. Seia	−3.0	153.0	multiple	225	Syn/Pre	N. Latona	bottom	45	37–51	-	-	37	30–48	5.0	9.5
8. Maram	−7.5	221.5	asymmetric	600	Syn/Pre	Parga	top	45	42–47	42	38–45	-	-	2.8	1.9
9.	3.5	233.7	concentric	225	Syn/Pre	Hecate	top	42	36–55	39	30–52	-	-	2.7	2.8
10. Chuku	−23.5	265.5	asymmetric	380	Syn/Pre	Parga	bottom	41	33–45	-	-	63	53–70	3.7	4.2
11. Hervor	−25.5	269.0	concentric-DR	250	Syn/Pre	Parga	bottom	41	31–47	-	-	53	44–59	1.8	5.2
12.	−22.8	259.6	multiple	380	Syn/Pre	Parga	bottom	32	0–40	-	-	52	34–60	1.7	4.1
13.	12.0	228.5	asymmetric	250	Syn/Pre	Hecate	top	31	26–36	52	46–61	-	-	4.0	2.6
14. Tadaka	−4.0	210.5	concentric	260	Syn/Pre	Parga	top	30	27–34	55	47–76	-	-	2.8	2.0
15. Nagavonyi	−18.5	259.0	multiple	225	Syn/Pre^{CZ}	Parga	top	0	0–5	41	36–45	-	-	7.5	3.8
16. Zisa	12.0	221.0	asymmetric	850	Syn/Pre	Hecate	top	0	0–5	61	59–65	-	-	2.3	1.0
17.	10.5	251.5	concentric	300	Syn	Hecate	top	48	44–52	30	29–42	-	-	1.0	1.4
18. Acrea	24.0	243.5	multiple	500	Syn^{CZ}	Hecate	top	22	14–27	62	57–73	-	-	4.8	3.2
19. Zamin	31.5	258.3	concentric	315	Syn^{CZ}	Hecate	top	2	0–14	56	46–67	-	-	2.5	4.2
20.	13.0	226.5	multiple	300	Syn^{HS}	Hecate	top	1	0–11	68	59–77	-	-	4.1	3.8
21. Erigone	−34.5	284.0	multiple	325	Syn	Parga	top	0	0–6	47	40–50	-	-	9.9	8.2
22.	31.5	255.0	concentric	300	Syn	Hecate-Asteria	top	0	0–10	62	51–69	-	-	3.3	3.9
23.	19.5	227.5	rad-concentric	350	Syn^{HS}	Hecate	top	0	0–5	49	46–54	-	-	7.0	1.5
24. Lengdin	2.5	223.0	asymmetric	518	Syn/Post	Hecate-Parga	top	35	29–39	37	34–43	-	-	2.9	1.2
25. Kapenopfu	−21.7	271.0	asymmetric	250	Syn/Post	Parga	top	24	22–27	6	3–9	-	-	6.3	4.3
26. Pazar-ana	−3.5	215.0	concentric-DR	300	Syn/Post	Parga	top	23	0–37	7	0–55	-	-	3.9	11.5
27. Perchta	17.0	234.5	rad-concentric	500	Syn/Post	Hecate	top	21	17–24	69	65–72	-	-	3.8	2.6
28. Obiemi	−31.9	276.6	asymmetric	300	Post	Parga	top	13	4–19	4	0–10	-	-	7.8	11.8
29.	22.0	224.0	rad-concentric	350	Post^{HS}	Hecate	top	12	8–13	48	47–53	-	-	1.1	0.8
30. Pani	19.9	231.5	concentric	320	Post^{HS}	Hecate	top	0	0–8	62	55–68	-	-	2.0	2.2
31. Mawu	31.7	241.3	concentric	385	Post	Hecate	top	0	0–10	63	51–69	-	-	3.3	3.9

[a]Maximum diameter from *Stofan et al.* [1992]. Superscript text denotes previously published relative timing interpretations. CZ, *Chapman and Zimbelman* [1998]; HS, *Hamilton and Stofan* [1996]. Quoted ranges of T_e, Z_c, and Z_L allow for RMS model misfit 1.5 times the observational RMS uncertainty.

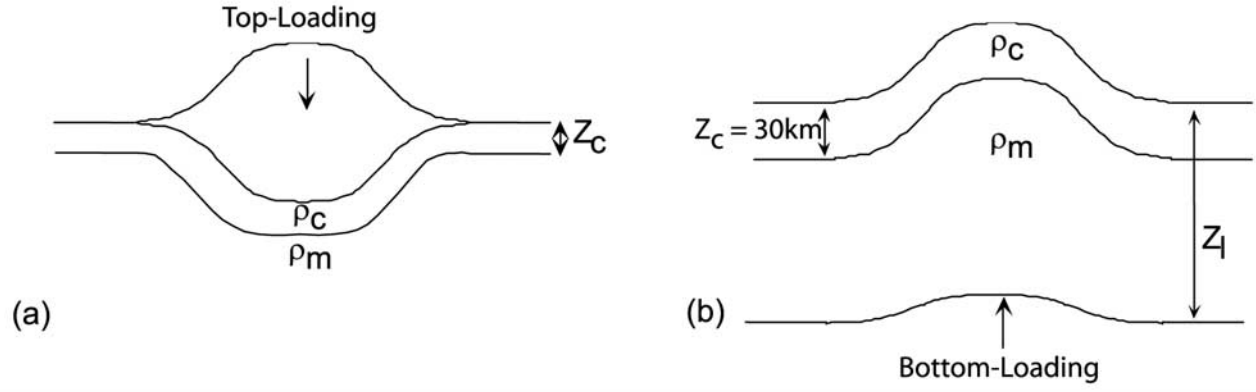

Figure 2. (a) Top- and (b) bottom-loading mechanical models are used to interpret the observed admittance functions of the Venusian lithosphere (depending on the shape of the observed admittance). Flexural analysis assumes a harmonically varying load, either (a) at the surface or (b) at a compensation depth below the crust-mantle interface. The top-loading model includes a crustal layer of thickness Z_c and elastic layer thickness T_e. The bottom-loading model includes a constant thickness crust and a second density interface at depth, Z_L, below the crust-mantle boundary. Apparent depth of compensation (Z_L) defines the depth above which the mass of the column is balanced with the load. Crustal (ρ_c) and mantle (ρ_m) densities of 2800 kg/m^3 and 3300 kg/m^3 are assumed in this analysis.

Hoogenboom et al. [2004]. The admittance was then interpreted using one of two loading models of the Venusian lithosphere (Figure 2). We assume the Venusian lithosphere has two laterally homogenous layers: crust of thickness Z_c overlying mantle to an apparent depth of compensation Z_L. Apparent depth of compensation (Z_L) defines the depth above which the load of the overlying mass is regionally balanced. Loaded by surface topography (top-loading) or by internal loads at depth Z_L (bottom-loading), the model lithosphere attains static equilibrium by elastic flexure of the uppermost elastic layer, thickness T_e [*Hoogenboom et al.*, 2004; *Smrekar et al.*, 2003]. By comparing the observed admittance spectra to the predictions of the two models, the effective elastic thickness is estimated. For the top-loading model (Figure 2a), Z_c is determined also, but the model admittance is independent of Z_L, which is therefore not determined. For the bottom-loading model (Figure 2b), Z_L and T_e are inferred from the admittance, assuming Z_c = 30 km [*Hoogenboom et al.*, 2004]. For a more detailed description of the model, the reader is referred to *Hoogenboom et al.* [2004].

2.2. Parameter Uncertainty

[8] Several factors contribute to the uncertainty in the estimated lithospheric parameters. These include data noise, method biases and the occurrence of processes other than flexural and isostatic adjustment of homogenous layers [*Smrekar et al.*, 2003]. *Banks et al.* [2001] described the impact of these factors on estimates of elastic thickness. *Lowry and Smith* [1995] discuss model parameter uncertainties calculated from terrestrial admittance studies. A further significant source of uncertainty arises from the lack of independent constraint on crustal thickness and density.

[9] We use the $1^\circ \times 1^\circ$ global admittance map of *Smrekar et al.* [2003] to evaluate an average admittance function for a square region centered on each corona, and extending far enough to cover all of the associated fractures. We estimate uncertainties following the approach adopted by *McKenzie and Fairhead* [1997]. For each corona, we estimate an observational uncertainty based on the variance of admittance within that region for each spectral component:

$$\sigma_l = \sqrt{\frac{\sum (x_l - \mu)^2}{N_{ADM}}}, \tag{1}$$

where the summation is over the N_{ADM} grid points in the corona region, x_l is the admittance at degree l and μ is the mean of the x_l values in that region. An average admittance uncertainty for each corona (Table 1, final column) is then defined by

$$\sigma = \frac{\sum \sigma_l}{N_l}, \tag{2}$$

where N_l is the number of degrees for which a compensation model is fit (usually l = 40 to 80 but variable depending on size of corona and local resolution of the gravity field). We then estimate uncertainty on the elastic model parameters by assuming that the RMS misfit between model admittance and average coronal admittance function is no greater than 1.5σ.

2.3. Relative Timing of Corona Formation

[10] Magellan stereo synthetic aperture radar (SAR) images are used in conjunction with full-resolution mosaic images ($\sim$100 to 250 m resolution) to interpret whether individual coronae associated with chasmata formed prior to, during, or after chasmata formation. The classification described by *Hamilton and Stofan* [1996] is used to categorize coronae on the basis of superposition and cross-cutting relationships between coronae and regional fractures and volcanism. Stratigraphic relationships are defined by the local stacking of geological features, with older below younger. Cross-cutting relationships may affect both mate-

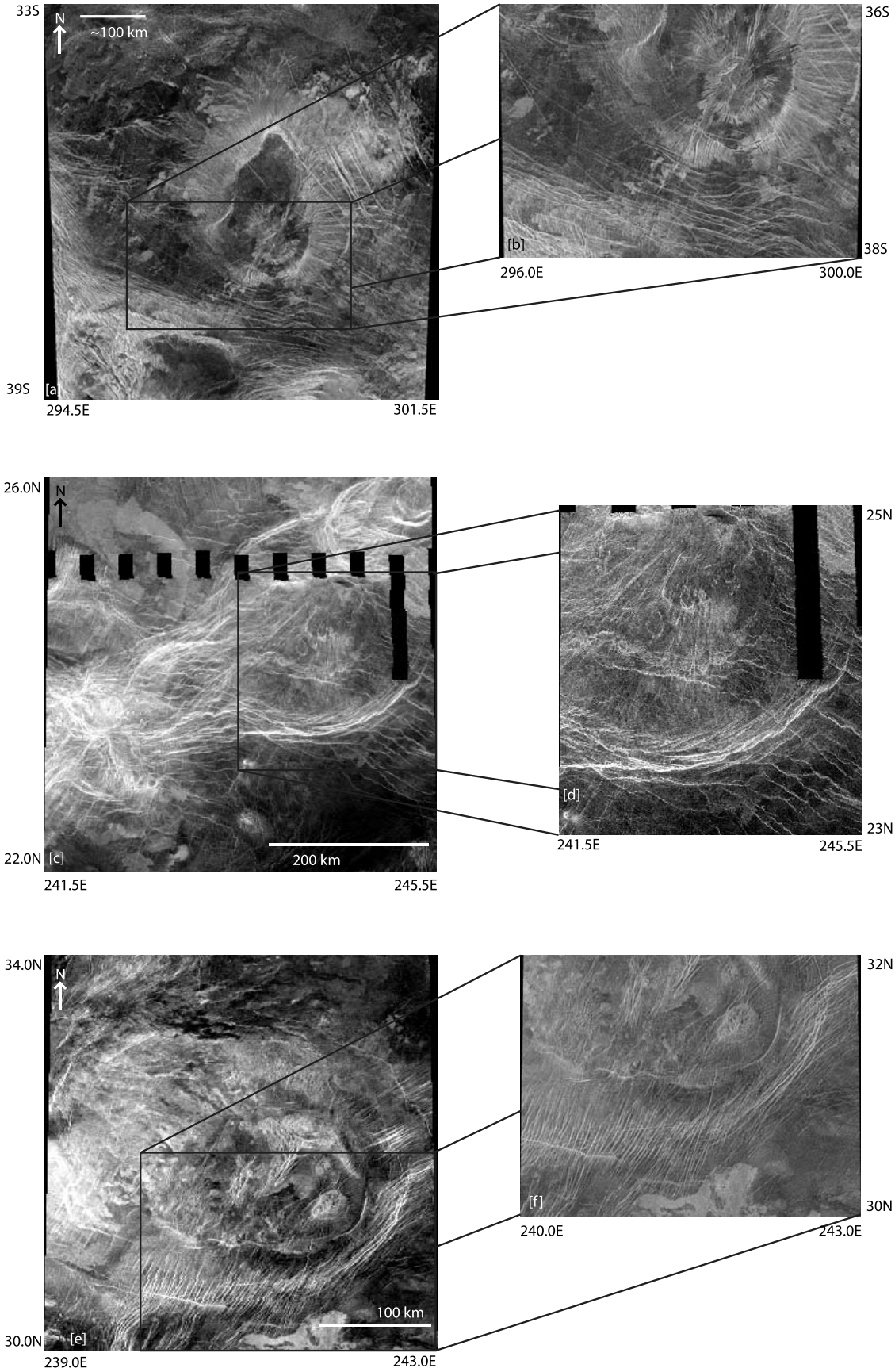
33S
N
~100 km
[a]
39S
294.5E
301.5E
36S
[b]
38S
296.0E
300.0E
26.0N
N
[c]
22.0N
200 km
241.5E
245.5E
25N
[d]
23N
241.5E
245.5E
34.0N
N
[e]
30.0N
100 km
239.0E
243.0E
32N
[f]
30N
240.0E
243.0E

Figure 3

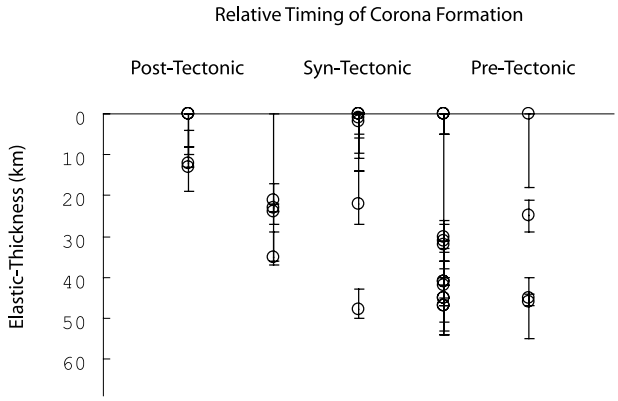

Figure 4. Elastic lithospheric thickness (T_e) as a function of the timing of corona formation relative to chasmata formation. Each individual corona (listed in Table 1) is represented by a circle. T_e estimates are obtained from the lithospheric parameter study of Type 1 coronae [*Hoogenboom et al.*, 2004]. Error bars represent the range of T_e values that provide an RMS misfit within a factor of 1.5 times the average uncertainty in the observed spectral admittance function [*Hoogenboom et al.*, 2004].

rial units and tectonic structures (e.g., fractures) and can provide relative age constraints for volcanic formations and tectonic structures such as fractures and faults that predate or postdate them. If regional fractures (fractures originating from the chasmata) terminate against the fracture sets associated with corona formation (e.g., a "T junction"), the corona-related fractures are presumed to be preexisting fractures that provide a structural barrier to the propagation of regional (chasmata-related) fractures. Furthermore, if regional fractures are deflected around a corona, the corona is again presumed to have formed first. In both cases, the corona is categorized as pretectonic (refer to Figures 3a and 3b). If regional (chasmata-related) fractures cut corona flows, and corona fractures or flows also superpose regional fractures, the corona is presumed to have formed at the same time (syntectonic) as the chasmata (Figures 1, 3c, and 3d). If regional (chasmata) fractures are clearly cross-cut by corona fractures, or hidden by corona flows, then the corona is classified as posttectonic [*Hamilton and Stofan*, 1996] (Figures 3e and 3f). Given the complexity of coronae-chasmata development, discussed below, two intermediate categories are also included: syntectonic/posttectonic and syntectonic/pretectonic (Table 1) [*Martin and Stofan*, 2004; *Martin et al.*, 2005].

[11] While numerous detailed mapping studies describe stratigraphic relationships between coronae and their surrounding geology [e.g., *Pronin and Stofan*, 1990; *Squyres et al.*, 1992; *Baer et al.*, 1994; *Chapman and Kirk*, 1996; *Hamilton and Stofan*, 1996; *Chapman and Zimbelman*, 1998; *Hansen and DeShon*, 2002], these studies use pre-Magellan or nonstereo data. Stereo imaging is critical to interpreting tectonic structures associated with coronae and the geologic sequence of events [*Ford et al.*, 1993], and allows the relationship between the chasmata trough and corona topography to be observed more clearly. As such, for all of the coronae examined in this paper, stereo images have been used in the interpretation of the relative timing relationships between coronae and chasmata formation.

[12] Despite the advantages of stereo data, determining the timing of corona formation relative to the surrounding units and tectonic structures is often complicated, and clear determinations have not been obtained for many corona. Often, coronae evolution involves multiple stages of volcanism, topographic uplift and fracture annulus formation [*Chapman and Zimbelman*, 1998; *Rosenberg and McGill*, 2001; *Hansen and DeShon*, 2002] therefore relative ages of individual tectonic structures or sets of structures may not accurately reflect the relative age of the corona as a whole. Tectonic structures can also be reactivated after their formation [*Hansen*, 2000]. Within these limitations, detailed stratigraphic mapping can be a reliable method of establishing the relative timing of corona formation [*Copp et al.*, 1998], when clear stratigraphic evidence is available.

[13] Given that coronae have formed at different times during the period recorded by Venus's present surface, and possibly have long and complex life spans [*Copp et al.*, 1998; *Rosenberg and McGill*, 2001; *Hansen and DeShon*, 2002], it is not possible to identify the relative ages of coronae within each class, only their timing of formation relative to the regional tectonism associated with chasmata formation.

3. Results

[14] Elastic thickness estimates for each corona are summarized in Table 1 with location, relative timing of formation, setting, diameter and annulus shape [*Stofan et al.*, 1992], crustal thickness, apparent depth of compensation and the flexural model used to calculate the lithospheric parameters. Of the 31 coronae examined here, the majority (26) were best fit with a top-loading model. The remaining 5 coronae were best fit with a bottom-loading model and classified as either pretectonic or syntectonic/pretectonic. Coronae that are best fit by a top-loading model are present in each of the relative timing groups. Elastic thickness for the 31 coronae examined here ranges from 0 to 56 km (including the range of error). These values lie within the

Figure 3. Magellan (left-looking) SAR images (sinusoidal projection) showing the relative timing relationships between coronae and their associated chasmata. (a) Tamiyo (36S, 298.5E) (resolution: 1.0 km/pixel), (c) Acrea (24N, 243.5E) (resolution: 1.2 km/pixel), and (e) Mawu (31.7N, 241.3E) (resolution: 1.2 km/pixel) coronae. Relative timing between individual coronae and their associated chasmata is established on the basis of superposition and cross-cutting relationships between coronae and regional fractures and volcanism. (b) Tamiyo (corona 1 in Table 1) is classified as pretectonic as regional fractures are deflected around Tamiyo (resolution: 0.5 km/pixel). (d) Acrea (corona 18 in Table 1) is classified as syntectonic as regional chasmata fractures cut corona flows, and corona fractures cut regional fractures (resolution: 0.6 km/pixel). (f) Mawu corona (corona 31 in Table 1) is classified as posttectonic as corona flows superpose regional fractures (resolution: 0.1 km/pixel). Black areas indicate regions with no data coverage.

range of previous elastic thickness estimates calculated for Venus [e.g., *Simons et al.*, 1997; *Barnett et al.*, 2000; *Smrekar et al.*, 2003] and Earth [e.g., *Watts et al.*, 1980].

[15] The relationship between elastic thickness and the relative timing of corona formation is shown in Figure 4. For the data available, the maximum elastic thickness in each group clearly increases from less than 20 km for posttectonic coronae to as much as 50 km for pretectonic coronae. Although coronae with small elastic thickness (<5 km) are found in all relative timing groups, the average value in each group increases along with the maximum.

[16] The majority of coronae analyzed here (~74%) formed synchronously with chasmata formation (i.e., classified as syntectonic/posttectonic, syntectonic, or syntectonic/pretectonic). Syntectonic/posttectonic coronae (four in total) exhibit elastic thickness estimates between 0 and 39 km (average 26 km ± 6 km). All of these coronae are best fit by a top loading model with best fit crustal thickness estimates ranging from 6 to 69 km (average 30 km ± 30 km). For syntectonic coronae (seven in total) display elastic thickness values up to 52 km (average 10 km ± 18 km). These coronae are fit by a top-loading model with best fit crustal thickness estimates ranging from 30 to 69 km (average 53 km ± 13 km). Elastic thickness estimates for coronae classified as syntectonic/pretectonic coronae (twelve in total) range between 0 and 56 km (average 33 km ± 17 km). For the eight coronae fit by a top-loading model the crustal thickness ranges from 39 to 61 km (average 48 km ± 8 km). For the 4 coronae fit with a bottom-loading model the best-fit compensation depth ranges from 37 to 63 km (average 51 km ± 11 km).

[17] The four coronae classified as posttectonic display small elastic thickness values: less than 19 km (average 6 km ± 7 km). All of these coronae are fit with a top-loading model, with crustal thickness estimates ranging from 4 to 63 km (average 44 km ± 28 km). Coronae that predate chasmata formation (four in total), display the largest range of elastic thickness values: between 0 and 56 km (average 29 km ± 22 km). The 3 of these that are best fit by a top-loading model have best-fit crustal thickness between 21 and 64 km (average 41 km ± 22 km). The other, fit with a bottom-loading model, has an apparent depth of compensation of 60 km.

[18] We find no clear correlation between diameter, annulus shape and relative timing of formation. *Martin et al.* [2005] examined 131 coronae located in the Parga Chasma region and also found no clear correlations between age, shape and size of coronae.

4. Discussion

[19] The majority of coronae analyzed here (~74%) formed synchronously with chasmata formation (i.e., classified as syntectonic/pretectonic, syntectonic, or syntectonic/posttectonic). For coronae located along Hecate Chasmata, *Stofan et al.* [1997] also found that chasmata formation and corona formation overlapped significantly in time. Using stereo images, *Martin and Stofan* [2004] found that a large number (85%) of the coronae associated with Parga Chasma are clearly active synchronous with rifting. *Hamilton and Stofan* [1996], however, found a roughly equal division among pretectonic, syntectonic, and posttectonic coronae along Hecate Chasma. These differences are ascribed to the use here of stereo images to interpret the age of coronae formation and the inclusion of two additional relative age classifications: syntectonic/posttectonic and syntectonic/pretectonic.

[20] Chasmata have previously been interpreted as extensional rift zones [*McGill et al.*, 1981; *Schaber*, 1982; *Solomon et al.*, 1992] similar to terrestrial rifts (such as East Africa) based on their lengths (hundreds to thousands of kilometers), widths (approximately hundreds of kilometers) and observed extension (tens of kilometers) [*McGill et al.*, 1981; *Foster and Nimmo*, 1996]. However, rifting on Venus appears to be predominantly related to convective upwelling in the mantle [e.g., *McGill et al.*, 1981] rather than plate motion. Impingement by a plume puts the lithosphere under stress [e.g., *Houseman and England*, 1986] and weakens it [*White and McKenzie*, 1989; *Saunders et al.*, 1992]. Injection of plume-related magma into the crust may then create a localized zone of weakness in which rifting occurs. Coronae that form subsequent to rifting (chasmata formation) therefore would develop in hotter, weaker lithosphere, and be associated with smaller values of T_e.

[21] A similar explanation for the relatively small elastic thickness estimates found in terrestrial studies of the East African rift is given by *Ebinger et al.* [1989]. Using the coherence between measured gravity and topography, *Ebinger et al.* [1989] determined effective elastic thicknesses and found the smallest elastic thicknesses (21 to 36 km) in the vicinity of severely faulted rift valleys. The reduced elastic thicknesses were attributed to mechanical weakening of the lithosphere due to heating involved in the rift formation process. In comparison they found that stable (colder) cratonic regions were found to be underlain by relatively thick elastic lithosphere (64 to 90+ km).

[22] Alternatively, small estimated values for coronae elastic thickness (<20 km) have been interpreted to represent an Airy-type isostatic compensation [*Johnson and Sandwell*, 1994; *Smrekar et al.*, 2003; *Hoogenboom et al.*, 2004], implying that flexural stresses created in the formation of these coronae are now relaxed for all wavelengths greater than the resolution of the Venusian gravity field (~300 km). In general, the elastic thickness of the terrestrial continental lithosphere has been suggested to increase with age since the last tectonic activity [*Haxby et al.*, 1976; *Molnar and Tapponnier*, 1981; *Karner et al.*, 1983]. However, this hypothesis cannot be tested on Venus, because absolute age determinations of coronae are not yet practical.

[23] To further constrain the origin and evolution of coronae and chasmata systems, *Martin et al.* [2005] have examined variations in other coronae characteristics (such as diameter, topography, annulus characteristics, associated volcanism and relative location) with respect to rifting along Parga Chasma.

5. Conclusions

[24] For the limited number of coronae examined in this study, smaller elastic thickness values (0 to 19 km) are found for coronae that formed after the chasmata with which they are associated. Coronae that formed before

chasmata formation display larger values of elastic thickness (0–56 km). These results suggest that coronae that form before chasmata formation may form on colder and stronger lithosphere and those that form after chasmata formation may form on weaker, less stable lithosphere. This interpretation is comparable with the interpretation of elastic layer thicknesses for the East African rift [*Ebinger et al.*, 1989]. While the results of this study indicate a correlation between elastic thickness and relative timing of the coronae examined, there remains no clear causal relationship between the formation and evolution of coronae and chasmata.

[25] Although only a small number of coronae were examined in this study due to low resolution of the Magellan gravity data in some regions of interest, the relationship between the local elastic thickness of the lithosphere and the relative ages of coronae appears valid. Improving the confidence of this result will await a higher-resolution, more complete model of the Venusian gravity field.

[26] **Acknowledgments.** We thank E. Stofan, A. Brian, and P. Grindrod for assistance with the Magellan stereo and FMAP data/interpretations. We also thank S. Smrekar, C. Ebinger, and J. Neuberg for valuable discussions and W. Kiefer, R. Ghent, and D. Jurdy for helpful and informative reviews. T.H. gratefully acknowledges financial support from the Royal Astronomical Society (London).

References

Baer, G., G. Schubert, D. L. Bindschadler, and E. R. Stofan (1994), Spatial and temporal relations between coronae and extensional belts, northern Lada-Terra, Venus, *J. Geophys. Res.*, *99*, 8355–8370.

Banks, R. J., S. C. Francis, and R. G. Hipkin (2001), Effects of loads in the upper crust on estimates of elastic thickness of the lithosphere, *Geophys. J. Int.*, *145*, 291–299.

Barnett, D. N., F. Nimmo, and D. McKenzie (2000), Flexure of Venusian lithosphere measured from residual topography and gravity, *Icarus*, *16*, 404–419.

Barnett, D. N., F. Nimmo, and D. McKenzie (2002), Flexure of Venusian lithosphere measured from residual topography and gravity, *J. Geophys. Res.*, *107*(E2), 5007, doi:10.1029/2000JE001398.

Barsukov, V. L., et al. (1984), Preliminary evidence on the geology of Venus from radar measurements by the Venera 16 and 16 probes, *Geokhimia*, *12*, 1811–1820. (*Geochem. Int. Engl. Transl.*, *22*, 135–143, 1985)

Chapman, M. G., and R. L. Kirk (1996), A migratory mantle plume on Venus: Implications for Earth?, *J. Geophys. Res.*, *101*(B7), 15,953–15,967.

Chapman, M. G., and J. R. Zimbelman (1998), Corona associations and their implications for Venus, *Icarus*, *32*, 344–361.

Copp, D. L., J. E. Guest, and E. R. Stofan (1998), Stratigraphy of six coronae on Venus: Implications for timing and sequence of corona formation, *J. Geophys. Res.*, *103*, 19,410–19,418.

Ebinger, C. J., T. D. Bechtel, D. W. Forsyth, and C. O. Bowin (1989), Effective elastic plate thickness beneath the East African and Afar Plateaus and dynamic compensation of the uplifts, *J. Geophys. Res.*, *94*, 2883–2901.

Ford, J. P., J. J. Plaut, C. M. Weitz, T. G. Farr, D. A. Senske, E. R. Stofan, G. Michaels, and T. J. Parker (1993), Guide to Magellan Image interpretation, *JPL Publ. 93-24*.

Foster, A. N., and F. Nimmo (1996), Comparison between the rift systems of East Africa, Earth and Beta Regio, Venus, *Earth Planet. Sci. Lett.*, *143*, 183–196.

Hamilton, V. E., and E. R. Stofan (1996), The geomorphology and evolution of Hecate Chasma, Venus, *Icarus*, *121*, 171–194.

Hansen, V. L. (2000), Geologic mapping of tectonic planets, *Earth Planet. Sci. Lett.*, *176*, 527–542.

Hansen, V. L. (2003), Venus diapirs: Thermal or compositional?, *Geol. Soc. Am. Bull.*, *115*(9), 1040–1052.

Hansen, V. L., and H. R. DeShon (2002), Geologic map of the Diana Chasma quadrangle (V-37), Venus, *U.S. Geol. Surv. Geol. Invest. Ser.*, *I-2752*, 1:5,000,000 scale, 1 sheet.

Hansen, V. L., and R. J. Phillips (1993), Tectonics and volcanism on Eastern Aphrodite Terra, Venus: No subduction, no spreading, *Science*, *260*, 526–530.

Hansen, V. L., J. J. Willis, and W. B. Banerdt (1997), Tectonic overview and synthesis, in *Venus II*, edited by S. W. Brougher, D. M. Hunten, and R. J. Phillips, pp. 797–844, Univ. of Ariz. Press, Tucson.

Haxby, W. F., D. L. Turcotte, and J. M. Bird (1976), Thermal and mechanical evolution of the Michigan basin, *Tectonophysics*, *36*, 57–75.

Hoogenboom, T., S. E. Smrekar, F. S. Anderson, and G. Houseman (2004), Admittance survey of type 1 coronae on Venus, *J. Geophys. Res.*, *109*, E03002, doi:10.1029/2003JE002171.

Houseman, G. A., and P. C. England (1986), A dynamical model of lithosphere extension and sedimentary basin formation, *J. Geophys. Res.*, *91*, 719–729.

Janes, D. M., S. W. Squyres, D. L. Bindschadler, G. Baer, G. Schubert, V. L. Sharpton, and E. R. Stofan (1992), Geophysical models for the formation and evolution of coronae on Venus, *J. Geophys. Res.*, *97*, 16,055–16,068.

Johnson, C. L., and D. T. Sandwell (1994), Lithospheric flexure on Venus, *Geophys. J. Int.*, *119*, 627–647.

Jurdy, D. M., and M. Stefanick (1999), Correlation of Venus surface features and geoid, *Icarus*, *139*, 93–99.

Karato, S. I., M. S. Paterson, and J. D. Fitzgerald (1986), Rheology of synthetic olivine aggregates: Influence of grain size and water, *J. Geophys. Res.*, *91*, 8151–8176.

Karner, G. D., M. S. Steckler, and J. A. Thorne (1983), Long term thermomechanical properties of the continental lithosphere, *Nature*, *304*, 250–253.

Koch, D. M., and M. Manga (1996), Neutrally buoyant diapirs: A model for Venus coronae, *Geophys. Res. Lett.*, *23*, 225–228.

Lowry, A. R., and R. B. Smith (1995), Strength and rheology of the western U.S. Cordillera, *J. Geophys. Res.*, *100*, 17,947–17,963.

Mackwell, S. J., and D. L. Kohlstedt (1993), High temperature deformation of diabase: Implications for tectonics on Venus, *Eos Trans. AGU*, *74*(43), Fall Meet. Suppl., 378.

Mackwell, S. J., M. E. Zimmerman, and D. L. Kohlstedt (1998), High-temperature deformation of dry diabase with application to tectonics on Venus, *J. Geophys. Res.*, *103*(B1), 975–984.

Martin, P., and E. R. Stofan (2004), Coronae of Parga Chasma, Venus, *Lunar Planet. Sci.*, *XXXV*, abstract 1576.

Martin, P., E. R. Stofan, and L. S. Glaze (2005), Analysis of coronae in the Parga Chasma region, *Venus, Lunar Planet. Sci.*, *XXXVI*, abstract 1617.

McGill, G. E., S. J. Steenstrup, C. Barton, and P. G. Ford (1981), Continental rifting and the origin of Beta Regio Venus, *Geophys. Res. Lett.*, *8*, 737–740.

McKenzie, D., and D. Fairhead (1997), Estimates of the effective elastic thickness of the continental lithosphere from Bouguer and free air gravity anomalies, *J. Geophys. Res.*, *102*(B12), 27,523–27,552.

McKenzie, D., P. J. Ford, C. Johnson, B. Parsons, D. Sandwell, S. Saunders, and S. C. Solomon (1992), Features on Venus generated by plate boundary processes, *J. Geophys. Res.*, *97*, 13,533–13,544.

Molnar, P., and P. Tapponnier (1981), A possible dependence of tectonic strength on the age of the crust in Asia, *Earth Planet. Sci. Lett.*, *52*, 107–114.

Pronin, A. A., and E. R. Stofan (1990), Coronae on Venus: Morphology, classification and distribution, *Icarus*, *87*, 452–474.

Rosenberg, E., and G. E. McGill (2001), Geologic map of the Pandrosos Dorsa (V5) quadrangle, Venus, *U.S. Geol. Surv. Geol. Invest. Map I-2721*, scale 1:5,000,000, 1 sheet.

Sandwell, D. T., and G. Schubert (1992), Evidence for retrograde lithospheric subduction on Venus, *Science*, *257*, 766–770.

Saunders, A. D., M. Storey, R. W. Kent, and M. J. Norry (1992), Consequences of plume-lithosphere interactions, in *Magmatism and the Causes of Continental Break-Up*, edited by B. C. Storey, T. Alabaster, and R. J. Pankhurst, *Geol. Soc. Spec. Publ.*, *68*, 41–60.

Schaber, G. G. (1982), Venus: Limited extension and volcanism along zones of lithospheric weakness, *Geophys. Res. Lett.*, *9*, 499–502.

Schubert, G., and D. T. Sandwell (1995), A global survey of possible subduction sites on Venus, *Icarus*, *117*, 173–196.

Senft, L., and W. S. Kiefer (2003), Crust and mantle structure of large coronae on Venus, *Lunar and Planet. Sci.*, *XXXIV*, abstract 1468.

Simons, M., S. C. Solomon, and B. H. Hager (1997), Localisation of gravity and topography: Constraints in the tectonics and mantle dynamics of Venus, *Geophys. J. Int.*, *131*, 24–44.

Smrekar, S. E., and E. R. Stofan (1997), Corona formation and heat loss on Venus by coupled upwelling and delamination, *Science*, *277*, 1289–1294.

Smrekar, S. E., R. Comstock, and F. S. Anderson (2003), A gravity survey of Type 2 coronae on Venus, *J. Geophys. Res.*, *108*(E8), 5090, doi:10.1029/2002JE001935.

Solomon, S. C., et al. (1992), Venus tectonics: An overview of Magellan observations, *J. Geophys. Res.*, *97*, 13,199–13,256.

Squyres, S. W., D. M. Janes, G. Baer, D. L. Bindschadler, G. Schubert, V. L. Sharpton, and E. R. Stofan (1992), The morphology and evolution of coronae on Venus, *J. Geophys. Res.*, *97*(E8), 13,611–13,634.

Stofan, E. R., D. L. Bindschadler, J. W. Head, and E. M. Parmentier (1991), Corona structures on Venus: Models of origin, *J. Geophys. Res.*, *96*, 20,933–30,946.

Stofan, E. R., V. L. Sharpton, G. Schubert, G. Baer, D. L. Bindschadler, D. M. Janes, and S. Squyres (1992), Global distribution and characteristics of coronae and related features on Venus: Implications for origin and relation to mantle processes, *J. Geophys. Res.*, *97*, 13,347–13,378.

Stofan, E. R., V. E. Hamilton, D. M. Janes, and S. E. Smrekar (1997), Coronae on Venus: Morphology and origin, in *Venus II*, edited by S. W. Brougher, D. M. Hunten, and R. J. Phillips, pp. 931–965, Univ. of Ariz. Press, Tucson.

Tackley, P. J., and D. J. Stevenson (1991), The production of small Venusian coronae by Rayleigh-Taylor instabilities in the uppermost mantle, *Eos Trans. AGU*, *72*(44), Fall Meet. Suppl., 287.

Watts, A. B., J. H. Bodine, and M. S. Steckler (1980), Observations of flexure and the state of stress in the oceanic lithosphere, *J. Geophys. Res.*, *85*(B11), 6369–6376.

White, R., and D. McKenzie (1989), Magmatism at rift zones: The generation of volcanic continental margins and flood basalts, *J. Geophys. Res.*, *94*, 7685–7729.

T. Hoogenboom, Jet Propulsion Laboratory, 4800 Oak Grove Drive, Mail Stop 183-501, Pasadena, CA 91106, USA. (trudi@jpl.nasa.edu)

G. Houseman, School of Earth and Environment, University of Leeds, Woodhouse Lane, Leeds LS2 9JT, UK.

P. Martin, Department of Physics, University of Cambridge, Madingley Road, Cambridge CB3 0HE, UK.